Estimation for Bridge Displacement at Different Sections through Data Fusion with Artificial Neural Network

Chenxi Wei
Department of Bridge Engineering, Tongji University, Shanghai, China; Shanghai Qizhi Institute, Shanghai, China; email: xichen@tongji.edu.cn

Limin Sun
Department of Bridge Engineering, Tongji University, Shanghai, China; Shanghai Qizhi Institute, Shanghai, China; email: lmsun@tongji.edu.cn

Ye Xia
Department of Bridge Engineering, Tongji University, Shanghai, China; Shanghai Qizhi Institute, Shanghai, China; email: yxia@tongji.edu.cn

Xuzhao Lu
Department of Bridge Engineering, Tongji University, Shanghai, China; Shanghai Qizhi Institute, Shanghai, China; email: luxuzhao_1992@tongji.edu.cn

Wei Zhang
Fujian Provincial Construction Engineering Quality Testing Center Co., LTD, Fujian Academy of Building Research Co., LTD, Fujian, China; email: fjjkyzw@163.com

ABSTRACT

Bridge displacement serves as a crucial parameter in bridge health monitoring. However, accurately measuring bridge displacement in practical engineering scenarios can be challenging due to terrain limitations. Scholars have proposed direct approaches, which utilize Linear Variable Displacement Transducers (LVDT), cameras, or millimeter-wave radars (MWR) for displacement measurement. However, these methods might be costly or fail to deliver satisfactory accuracy, especially in adverse weather conditions. Consequently, recent years have seen the emergence of indirect approaches employing strain gauges or accelerometers for bridge displacement estimation. However, these indirect methods necessitate certain pre-known information about the target bridge or moving vehicle, such as the vertical distance between the sensor and the central axis, which can be difficult to acquire. In this study, a novel bridge displacement estimation method is proposed through data fusion with a machine learning method. In addition to accelerations at multiple cross-sections, displacements at some specific locations are also measured. Theoretical derivations of bridge dynamics suggest the feasibility of combining measured displacement and acceleration to estimate displacement across all cross-sections. Subsequently, the Artificial Neural Network (ANN) method is employed to train a model corresponding to the mapping between bridge accelerations at different cross-sections, which takes advantage of machine learning methods in de-noise in comparison to traditional methods. This model is then utilized for bridge displacement estimation. Furthermore, finite element simulation was processed to validate the proposed method.

KEYWORDS: Bridge displacement estimation; Data fusion; Artificial Neural Network

1. INTRODUCTION

Bridge displacement measurement is a crucial aspect of bridge health monitoring, involving bridge damage detection (Ge et al., 2023) and bridge weight-in-motion (B-WIM) (Kim et al., 2022). For short- and medium-span bridges, significant deflection is caused by moving vehicles, making the measurement of bridge displacement under vehicle loads a widely researched topic.

Bridge displacement measurement methods are generally classified into direct and indirect approaches. Direct methods involve devices that directly capture real-time bridge deflection, such as Linear Variable Differential Transformers (LVDT) (Peddle et al., 2011), Laser Doppler Vibrometers (LDV) (Garg et al., 2019), and millimeter-wave radar (Michel and Keller, 2021). However, these techniques often require costly equipment. Although vision-based measurement approaches (Nasimi and Moreu, 2021) have been proposed as relatively cheaper alternatives, they struggle to maintain high accuracy under adverse weather conditions like fog, snow, or heavy rain.

In contrast, indirect methods use more affordable sensors to estimate bridge displacement from monitored bridge response data. A common method employs accelerometers (Gindy et al., 2007), where the time history of bridge displacement is derived through double integration of the acceleration data. However, in practical applications, the measured bridge acceleration signal often contains unknown environmental and measurement noise (Gindy et al., 2008, Nagayama and Zhang, 2017). Additionally, the initial state of the bridge is typically unknown, leading to direct double integration to produce unrealistic drifting displacement. While some researchers have suggested processing bridge acceleration using Tikhonov regularization (Park et al., 2005), and even more advanced methods (Park et al., 2013) that combine acceleration and strain data, these methods require the vertical distance between the measuring location and the central axis of the corresponding cross-section as known information, which is also hard to be determined for actual bridges.

This study proposes a novel indirect method to estimate bridge displacement under vehicle loading. To solve the above shortcomings of the indirect methods, we combined the bridge acceleration data from multiple locations and the bridge displacement data from some of these locations to estimate the displacement at other locations. This method is grounded in the physical characteristics of bridge dynamics in vehicle-bridge-interaction (VBI) systems (Kim et al., 2005). It was found that the transfer function for acceleration between multiple locations, and the transfer function of displacement between multiple locations are the same. Using Back-Propagation Artificial Neural Network (BP-ANN) (Huang et al., 2022) for de-noising, we simulated the transfer function corresponding to high-frequency bridge acceleration. This function enables the estimation of bridge displacement. Consequently, once the displacement at certain easily accessible locations is measured, the displacement at other locations can be estimated. Compared to existing indirect methods, our approach does not require knowledge of the distance to the central axis and is more applicable in real engineering scenarios.

This paper first illustrates the theoretical background of bridge dynamics in a simple VBI system and introduces the basics of the BP-ANN network. A series of finite element simulations validate the proposed method.

2. METHODOLOGY

2.1. *Dynamics of Simple VBI System*

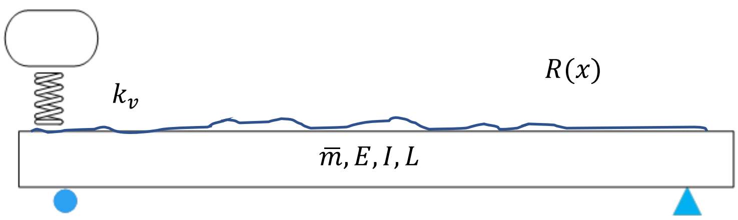

Figure 1 A simple VBI system

A typical VBI system consists of a simply supported beam and the moving single degree of freedom sprung mass (shown in Fig. 1). As Yang derived in (Yang and Lin, 2005), the dynamic equation of the vehicle in the VBI system is shown in Eq. (1) and Eq. (2) as,

$$\mathrm{m_v\ddot{u}_v(t) + k_v[u_v(t)\text{-}u_w(t)] = 0} \tag{1}$$

$$u_w(t) = u_b(x,t)|_{x=vt} + R(x)|_{x=vt} \tag{2}$$

where $u_v(t)$ and $\ddot{u}_v(t)$ represent the vertical displacement and acceleration of the sprung mass. $u_w(t)$ stands for the vertical displacement of the contact point. m_v and k_v are the vehicle mass and the spring stiffness, and $R(x)$ is the road roughness at the location x; v signifies the vehicle speed.

The dynamic equation of the bridge in the VBI system is shown in Eq. (3).

$$\bar{m}\ddot{u}_b(x,t) + EIu_b''''(x,t) = \{k_v[u_v(t) - (u_b(x,t)|_{x=vt} + R(x)|_{x=vt})] - m_v g\}\delta(x - vt) \tag{3}$$

Considering that road roughness has a very limited impact on bridge dynamic responses, its potential influence is neglected in this study. Furthermore, as Yang stated, when the vehicle mass is much smaller than the bridge mass, the influence of the moving vehicle can be simplified to a moving force equal to the gravitational force of the sprung mass $m_v g$. Thus, the dynamic displacement of the bridge can be solved as follows (Eq. (4), Eq. (5)).

$$u(x,t) = \sum_n \frac{\Delta_{stn}}{1 - S_n^2}\{sin\frac{n\pi x}{L}[\sin\frac{n\pi vt}{L} - S_n \sin\omega_{bn}t]\} \tag{4}$$

Where,

$$\Delta_{st,n} = \frac{-2m_v g L^3}{n^4\pi^4 EI} \tag{5.a}$$

$$S_n = \frac{n\pi v}{L\omega_{b,n}} \tag{5.b}$$

$$\omega_{b,n} = \frac{n^2\pi^2}{L^2}\sqrt{\frac{EI}{\bar{m}}} \tag{5.c}$$

The $u(x,t)$ in Eq. (4) consists of a low-frequency part $u_{low}(x,t)$ and a high-frequency part $u_{high}(x,t)$ (shown in Eq. (6)).

$$u_{low}(x,t) = \sum_n \frac{\Delta_{stn}}{1 - S_n^2}[sin\frac{n\pi x}{L}sin\frac{n\pi vt}{L}] \tag{6.a}$$

$$u_{high}(x,t) = \sum_n \frac{\Delta_{stn}}{1 - S_n^2}[-sin\frac{n\pi x}{L}S_n \, sin\,\omega_{b,n}t] \tag{6.b}$$

2.2. *Data Fusion Mechanism Between Bridge Acceleration and Bridge Displacement*

Assume that there are three cross-sections x_1, x_2, and x_3, this study aims to use the acceleration at all these cross-sections and the displacement at x_1 and x_2 to estimate the displacement at x_3. High-frequency acceleration at x_1 is shown in Eq. (7).

$$\ddot{u}_{high}(x,t) = \sum_n \frac{\Delta_{stn}}{1 - S_n^2}{\omega_{b,n}}^2\left[sin\frac{n\pi x}{L}S_n \, sin\,\omega_{b,n}t\right] \tag{7}$$

Then the following equation can be derived as follow (Eq. (8)).

$$\begin{bmatrix} sin\frac{\pi x_1}{L} & sin\frac{2\pi x_1}{L} & \cdots & sin\frac{n\pi x_1}{L} \\ sin\frac{\pi x_2}{L} & sin\frac{2\pi x_2}{L} & \cdots & sin\frac{n\pi x_2}{L} \\ sin\frac{\pi x_3}{L} & sin\frac{2\pi x_3}{L} & \cdots & sin\frac{n\pi x_3}{L} \end{bmatrix}$$

$$
\begin{bmatrix}
\frac{\Delta_{st,1}}{1-S_1^2}\omega_{b,1}{}^2 S_1 sin\omega_{b,1}t_0 & \frac{\Delta_{st,1}}{1-S_1^2}\omega_{b,1}{}^2 S_1 sin\omega_{b,1}t_1 & \cdots & \frac{\Delta_{st,1}}{1-S_1^2}\omega_{b,1}{}^2 S_1 sin\omega_{b,1}t_N \\
\frac{\Delta_{st,2}}{1-S_2^2}\omega_{b,2}{}^2 S_2 sin\omega_{b,2}t_0 & \frac{\Delta_{st,2}}{1-S_2^2}\omega_{b,1}{}^2 S_2 sin\omega_{b,2}t_1 & \cdots & \frac{\Delta_{st,2}}{1-S_2^2}\omega_{b,1}{}^2 S_2 sin\omega_{b,2}t_N \\
\vdots & \vdots & \vdots & \vdots \\
\frac{\Delta_{st,n}}{1-S_n^2}\omega_{b,n}{}^2 S_n sin\omega_{b,n}t_0 & \frac{\Delta_{st,n}}{1-S_n^2}\omega_{b,n}{}^2 S_n sin\omega_{b,n}t_1 & \cdots & \frac{\Delta_{st,n}}{1-S_n^2}\omega_{b,n}{}^2 S_n sin\omega_{b,n}t_N
\end{bmatrix}
= \begin{bmatrix}
\ddot{u}_{x_1,t_0} & \ddot{u}_{x_1,t_1} & \cdots & \ddot{u}_{x_1,t_N} \\
\ddot{u}_{x_2,t_0} & \ddot{u}_{x_2,t_1} & \cdots & \ddot{u}_{x_2,t_N} \\
\ddot{u}_{x_3,t_0} & \ddot{u}_{x_3,t_1} & \cdots & \ddot{u}_{x_3,t_N}
\end{bmatrix}_{high} \tag{8}
$$

If only the first two vibration modes were included, the following equation can be derived as follows (Eq. (9), Eq. (10)).

$$
\begin{bmatrix}
\ddot{u}_{x_2,t_0} & \ddot{u}_{x_2,t_1} & \cdots & \ddot{u}_{x_2,t_N} \\
\ddot{u}_{x_3,t_0} & \ddot{u}_{x_3,t_1} & \cdots & \ddot{u}_{x_3,t_N}
\end{bmatrix}
= \boldsymbol{T}
\begin{bmatrix}
\ddot{u}_{x_1,t_0} & \ddot{u}_{x_1,t_1} & \cdots & \ddot{u}_{x_1,t_N} \\
\ddot{u}_{x_2,t_0} & \ddot{u}_{x_2,t_1} & \cdots & \ddot{u}_{x_2,t_N}
\end{bmatrix} \tag{9}
$$

where

$$
\boldsymbol{T} = \begin{bmatrix}
sin\frac{\pi x_2}{L} & sin\frac{2\pi x_2}{L} \\
sin\frac{\pi x_3}{L} & sin\frac{2\pi x_3}{L}
\end{bmatrix}
\begin{bmatrix}
sin\frac{\pi x_1}{L} & sin\frac{2\pi x_1}{L} \\
sin\frac{\pi x_2}{L} & sin\frac{2\pi x_2}{L}
\end{bmatrix}^{-1} \tag{10}
$$

Similarly, the low-frequency displacement at three cross-sections can be calculated as follows (Eq. (11), Eq. (12), Eq. (13)).

$$
\begin{bmatrix}
sin\frac{\pi x_1}{L} & sin\frac{2\pi x_1}{L} & \cdots & sin\frac{n\pi x_1}{L} \\
sin\frac{\pi x_2}{L} & sin\frac{2\pi x_2}{L} & \cdots & sin\frac{n\pi x_2}{L} \\
sin\frac{\pi x_3}{L} & sin\frac{2\pi x_3}{L} & \cdots & sin\frac{n\pi x_3}{L}
\end{bmatrix}
\begin{bmatrix}
\frac{\Delta_{st,1}}{1-S_1^2} sin\frac{\pi v t_0}{L} & \frac{\Delta_{st,1}}{1-S_1^2} sin\frac{\pi v t_1}{L} & \cdots & \frac{\Delta_{st,1}}{1-S_1^2} sin\frac{\pi v t_N}{L} \\
\frac{\Delta_{st,2}}{1-S_2^2} sin\frac{2\pi v t_0}{L} & \frac{\Delta_{st,2}}{1-S_2^2} sin\frac{2\pi v t_1}{L} & \cdots & \frac{\Delta_{st,2}}{1-S_2^2} sin\frac{2\pi v t_N}{L} \\
\vdots & \vdots & \vdots & \vdots \\
\frac{\Delta_{st,n}}{1-S_n^2} sin\frac{n\pi v t_0}{L} & \frac{\Delta_{st,n}}{1-S_n^2} sin\frac{n\pi v t_1}{L} & \cdots & \frac{\Delta_{st,n}}{1-S_n^2} sin\frac{n\pi v t_N}{L}
\end{bmatrix}
= \begin{bmatrix}
u_{x_1,t_0} & u_{x_1,t_1} & \cdots & u_{x_1,t_N} \\
u_{x_2,t_0} & u_{x_2,t_1} & \cdots & u_{x_2,t_N} \\
u_{x_3,t_0} & u_{x_3,t_1} & \cdots & u_{x_3,t_N}
\end{bmatrix} \tag{11}
$$

And,

$$
\begin{bmatrix}
u_{x_2,t_0} & u_{x_2,t_1} & \cdots & u_{x_2,t_N} \\
u_{x_3,t_0} & u_{x_3,t_1} & \cdots & u_{x_3,t_N}
\end{bmatrix}
= \boldsymbol{T'}
\begin{bmatrix}
u_{x_1,t_0} & u_{x_1,t_1} & \cdots & u_{x_1,t_N} \\
u_{x_2,t_0} & u_{x_2,t_1} & \cdots & u_{x_2,t_N}
\end{bmatrix} \tag{12}
$$

Where,

$$
\boldsymbol{T'} = \begin{bmatrix}
sin\frac{\pi x_2}{L} & sin\frac{2\pi x_2}{L} \\
sin\frac{\pi x_3}{L} & sin\frac{2\pi x_3}{L}
\end{bmatrix}
\begin{bmatrix}
sin\frac{\pi x_1}{L} & sin\frac{2\pi x_1}{L} \\
sin\frac{\pi x_2}{L} & sin\frac{2\pi x_2}{L}
\end{bmatrix}^{-1} \tag{13}
$$

It can be found following (Eq. (14)),

$$
\boldsymbol{T} = \boldsymbol{T'} \tag{14}
$$

2.3. *BP-ANN*

Since the transfer functions corresponding to acceleration and displacement are the same, once the transfer function between accelerations at different cross-sections is identified, the displacement at a specific cross-section can be estimated using the same function. In this study, the transfer function is identified through a BP-ANN.

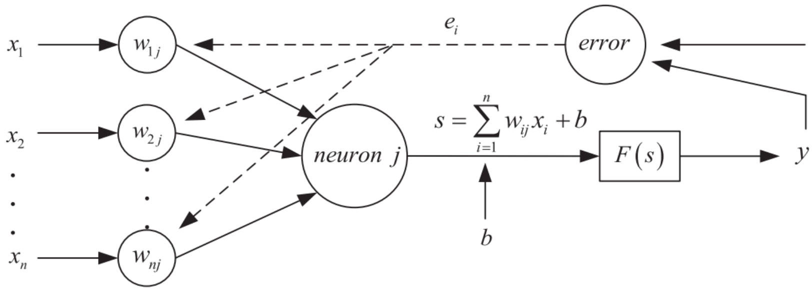

Figure 2 Artificial neuron unit (Huang et al., 2022)

A typical back-propagation neural network structure (Huang et al., 2022) consists of artificial neuron units, as shown in Figure 2, where $x_i(i=1,2,\dots n)$ denotes the input of the current unit j. w_{ij} is the corresponding weight to each input. Then the output *y* of the unit *j* is calculated as follows (Eq. (15)).

$$s=\sum_{i=1}^{n} w_{ij}x_i+b \tag{15.a}$$

$$y=F(s)=\frac{1}{1+e^{-s}} \tag{15.b}$$

in which *b* is the bias term.

Back-propagation neural networks are composed of input layers, output layers, and hidden layers. Each layer consists of one or more artificial neuron units. During training, these units receive output from the previous layer and calculate input for the next layer. The weights and biases are adjusted iteratively to minimize the total error, according to Eq. (16), Eq. (17), and Eq. (18) (Huang et al., 2022):

$$w(k+1)=w(k)-\alpha\frac{\partial E(k)}{\partial w(k)} \tag{16}$$

$$b(k+1)=b(k)-\alpha\frac{\partial E(k)}{\partial b(k)} \tag{17}$$

in which,

$$E(k)=\sqrt{\frac{1}{N}\sum_{i=1}^{N}|e_i|^2} \tag{18}$$

The $w(k+1)$ and $b(k+1)$ are the weight and bias of the (*k*+1)-*th* iteration, respectively; α is the learning rate. *E* is the function of the total error of the output, and e_i denotes the error between the true value and the simulated result.

3. VALIDATION WITH FINITE ELEMENT SIMULATION

3.1. *Numerical Model*

In this study, two finite element models (FEM) were employed to generate training and test data for the ANN. These models are simple VBI systems comprising a simply supported bridge and a sprung-mass vehicle. The parameters for the bridge and vehicle are detailed in Tables 1 and 2, respectively.

Table 1 Bridge parameters

Parameters	Values
Span Length (m)	25
Density (kg/m^3)	3598.44
Young's Modulus (GPa)	287
Poisson's Ratio	0.2

Table 2 Vehicle parameters

Parameters	Values
Velocity (m/s)	1
Density (kg/m^3)	11230(Model 1)/10500(Model 2)
Young's Modulus (GPa)	287
Poisson's Ratio	0.2

The vehicle traveled steadily across the entire span of the bridge at a velocity of 1 m/s. The finite element method computed the dynamic response of the system, with an analytical time step of 0.01 s. Nodes near the quarter, one-third, half, and three-quarter spans of the bridge were randomly selected, and their acceleration and vertical displacement were extracted to create datasets for the neural network. By altering the vehicle's density, Model 2 was created, and the same steps were repeated to obtain acceleration and vertical displacement data, thereby expanding the datasets.

3.2. *ANN Training*

Using the FEM simulations described above, datasets for the neural network were obtained. One dataset consists of acceleration data (input) from nodes A (near 1/4 span), B (near 1/2 span), and C (near 3/4 span) at specific moments, and acceleration data (output) from node D (near 1/3 span), totaling 5024 datasets. These datasets were randomly divided into training and testing sets, with the testing set comprising 20% of the total. To simulate measurement and environmental noise, Gaussian white noise with a mean of 0 and a standard deviation of 10^{-4} m/s^{-2} was added to the three sets of acceleration data at the input layer.

Subsequently, a model was trained using the datasets to estimate the acceleration of node D based on the acceleration data from nodes A, B, and C. The BP-ANN structure adopted in this study includes one hidden layer with four neurons. The learning rate was set to 0.001, and the epoch was set to 100,000. Mean square error was used as the loss function. The training performance of the model is shown in Figure 3.

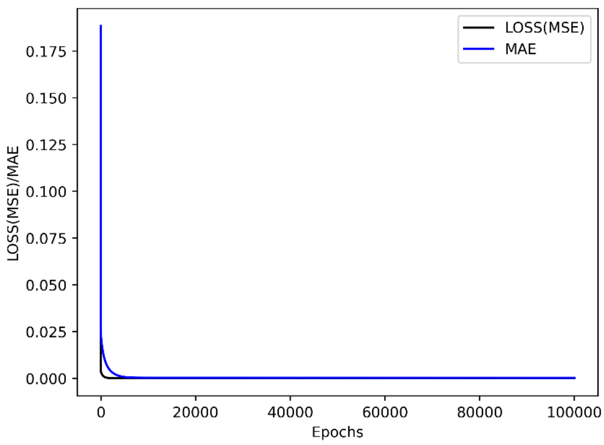

Figure 3 Loss (mean squared error) and mean absolute error (MAE)

3.3. *Bridge Displacement Estimation*

The trained model was then utilized for bridge displacement estimation. To simulate measurement and environmental noise, Gaussian white noise with a mean of 0 and a standard deviation of 10^{-4} m was added to the vertical displacement data of nodes A, B, and C. These noisy vertical displacement data were used as input features to predict the vertical displacement of node D using the trained model.

The vertical displacement reconstruction of node D was completed using the trained BP-ANN model. Figures 4 and 5 display the time history of the vertical displacement of node D. To filter out noise, a low-pass filter with a cutoff frequency of 1 Hz was employed. Finally, the comparison between the reconstructed and true vertical displacements of node D is shown in Figures 6 and 7. The results demonstrate that the estimated displacement matches well with the true values.

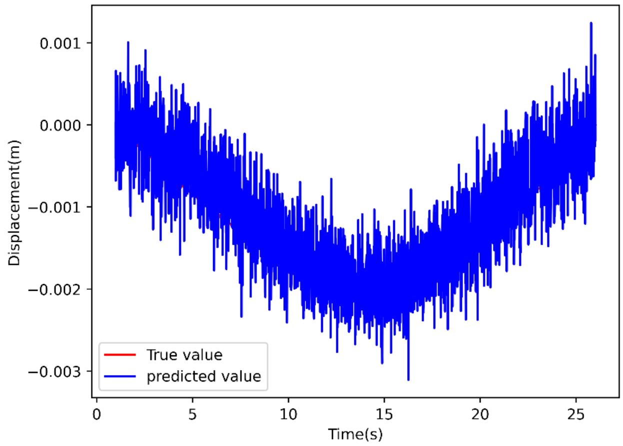

Figure 4 The predicted vertical displacement of Node D (Model 1)

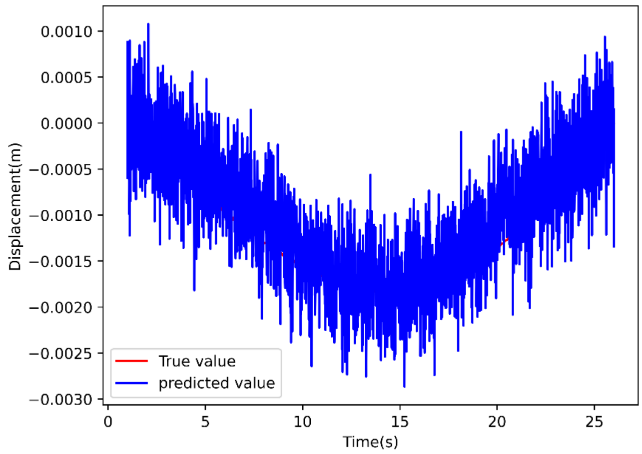

Figure 5 The predicted vertical displacement of Node D (Model 2)

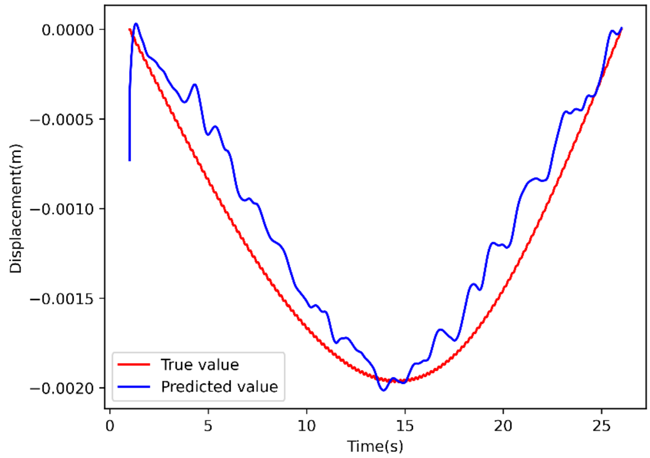

Figure 6 Reconstruction results of the vertical displacement of Node D (Model 1)

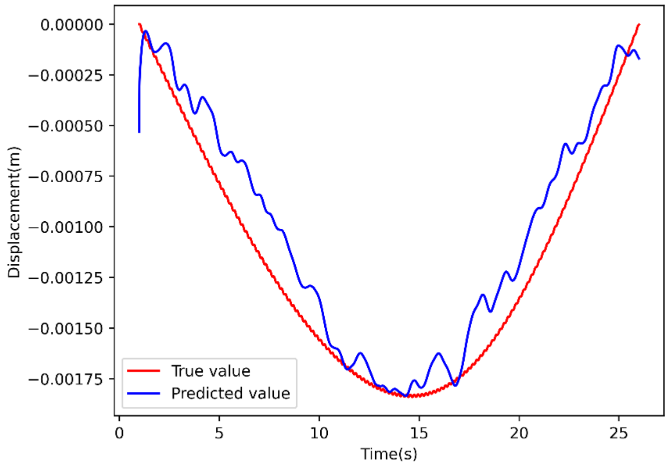

Figure 7 Reconstruction results of the vertical displacement of Node D (Model 2)

4. CONCLUSIONS

In this study, a novel method is proposed to estimate bridge displacement under vehicle loading at some specification by merging bridge acceleration data from multiple locations with bridge displacement data from some of these locations. Two major conclusions can be drawn:

(1) Theoretical analysis of bridge dynamics in a simple VBI system indicates that the transfer function for bridge acceleration at multiple locations and the transfer function for bridge displacement at multiple locations are identical, despite the different units of acceleration and displacement.

(2) The application of BP-ANN demonstrates promising results for bridge displacement estimation at specific locations.

While the estimation results appear good in numerical simulations, it is important to note an implicit prerequisite: the training input data for the BP-ANN should encompass major vibration modes corresponding to the output training data. For bridge structures with multiple significant vibration modes, it is necessary to identify key cross-sections to capture sufficient mode shape information. This issue will be discussed in future studies.

ACKNOWLEDGEMENTS

This paper is supported by National Natural Science Foundation of China (NO. 52411540031), the Technology Cooperation Project of Shanghai Qizhi Institute (NO. SQZ202310) and Science and Technology Project by Department of housing and urban rural development of Fujian Province, China (NO. 2023Y0040).

REFERENCES

Garg, P., Moreu, F., Ozdagli, A., Taha, M.R. and Mascareñas, D. 2019. Noncontact dynamic displacement measurement of structures using a moving laser Doppler vibrometer. *Journal of Bridge Engineering*, 24(9), 04019089.

Ge, L., Koo, K. Y., Wang, M., Brownjohn, J. and Dan, D. 2023. Bridge damage detection using precise vision-based displacement influence lines and weigh-in-motion devices: Experimental validation. *Engineering Structures*, 288, 116185.

Gindy, M., Nassif, H.H. and Velde, J. 2007. Bridge displacement estimates from measured acceleration records. *Transportation Research Record: Journal of the Transportation Research Board*, 2028(1), 136–145.

Gindy, M., Vaccaro, R., Nassif, H. and Velde, J. 2008. A state-space approach for deriving bridge displacement from acceleration. *Computer-Aided Civil and Infrastructure Engineering*, 23(4), 281–290.

Huang, L., Chen, J. and Tan, X. 2022. BP-ANN based bond strength prediction for FRP reinforced concrete at high temperature. *Engineering Structures, 257*, 114026.

Kim, C. W., Kawatani, M. and Kim, K.B. 2005. Three-dimensional dynamic analysis for bridge–vehicle interaction with roadway roughness. *Computers & Structures*, 83(19–20), 1627–1645.

Kim, S.-W., Yun, D.-W., Park, D.-U., Chang, S.-J. and Park, J.-B. 2022. Vehicle load estimation using the reaction force of a vertical displacement sensor based on fiber Bragg grating. *Sensors*, 22(4), 1572.

Michel, C. and Keller, S. 2021. Advancing ground-based radar processing for bridge infrastructure monitoring. *Sensors*, 21(6), 2172.

Nagayama, T. and Zhang, C. 2017. Deflection estimation of a steel box girder bridge using multi-channel acceleration measurement. *In IABSE Symposium: Engineering the Future, Vancouver, Canada, 21-23 September 2017* (pp. 1667-1674).

Nasimi, R. and Moreu, F. 2021. A methodology for measuring the total displacements of structures using a laser–camera system. *Computer-Aided Civil and Infrastructure Engineering*, 36(4), 421–437.

Park, J.-W., Sim, S.-H. and Jung, H.-J. 2013. Displacement estimation using multimetric data fusion. *IEEE/ASME Transactions on Mechatronics*, 18(6), 1675–1682.

Park, K.-T., Kim, S.-H., Park, H.-S. and Lee, K.-W. 2005. The determination of bridge displacement using measured acceleration. *Engineering Structures*, 27(3), 371–378.

Peddle, J., Goudreau, A., Carlson, E. and Santini-Bell, E. 2011. Bridge displacement measurement through digital image correlation. *Bridge Structures*, 7(4), 165–173.

Yang, Y. B. and Lin, C. W. 2005. Vehicle–bridge interaction dynamics and potential applications. Journal of Sound and Vibration, 284(1–2), 205–226.